Nonaffine heterogeneities and droplet fluctuations in an equilibrium crystalline solid

Tamoghna Das,[1,*] Surajit Sengupta,[2,1,3,†] and Madan Rao[4,5,3,‡]
[1]*Advanced Materials Research Unit, S. N. Bose National Centre for Basic Sciences, Salt Lake, Kolkata 700091, India*
[2]*Centre for Advanced Materials, Indian Association for the Cultivation of Science, Jadavpur, Kolkata 700032, India*
[3]*Kavli Institute for Theoretical Physics, UCSB, Santa Barbara, California 93106-4030, USA*
[4]*Raman Research Institute, C.V. Raman Avenue, Bangalore 560080, India*
[5]*National Centre for Biological Sciences (TIFR), Bellary Road, Bangalore 560065, India*
(Received 14 July 2010; revised manuscript received 2 September 2010; published 19 October 2010)

We show, using molecular-dynamics simulations, that a two-dimensional Lennard-Jones solid exhibits droplet fluctuations characterized by *nonaffine* deviations from local crystallinity. The fraction of particles in these droplets increases as the mean density of the solid decreases and approaches ≈20% of the total number in the vicinity of the fluid-solid phase boundary. We monitor the geometry, local equation of state, density correlations, and Van Hove functions of these droplets. We provide evidence that these nonaffine heterogeneities should be interpreted as being droplet fluctuations from nearby metastable minima. The local excess pressure of the droplets plotted against the local number density shows a van der Waal loop with distinct branches corresponding to fluidlike compact and stringlike glassy droplets. The distinction between fluidlike and glassy droplets disappears above a well-defined temperature.

DOI: 10.1103/PhysRevE.82.041115 PACS number(s): 64.60.My, 64.70.D−, 64.70.Q−, 81.05.Kf

I. INTRODUCTION

Crystalline solids typically exhibit local nonaffine deformations when driven by external stresses. In many instances these nonaffine deformations can be described in terms of a density of dislocations; however, such a description is problematic when the density of dislocations is large enough that their cores overlap [1]. Since the overlapping cores of the dislocations have the character of a fluid, it has been suggested that these excitations should be thought of as fluidlike droplets [2–5]. This has proved a useful interpretation, especially since amorphous solids, for which dislocations are difficult to define, also show such localized deformations under shear.

Just as dislocations in a solid can be thermally excited in the absence of external drive, it is reasonable to ask whether these fluidlike droplet fluctuations [6] can arise in the absence of external perturbation, especially when close to the fluid-solid phase boundary. Droplet fluctuations have been studied in great detail for simple Ising systems undergoing a first-order transition where they are known to influence the asymptotic behavior of dynamic correlations and introduce subtle essential singularities in the equilibrium free energy [7]. The nature and role of droplet fluctuations in solids, on the other hand, has not received similar attention. In this paper, using a molecular-dynamics (MD) simulation of a two-dimensional (2D) Lennard-Jones (LJ) solid, we show that, indeed, thermally excited droplet fluctuations do exist close to melting. We characterize the local droplet fluctuations using a nonaffine order parameter [8] and further classify them as being fluidlike or "glassy" (reflecting the whole family of noncrystalline metastable configurations).

We report MD simulations of a 2D single-component system with the atoms interacting via LJ potential, viz.,

$$\phi(r) = 4\epsilon[(\sigma/r)^{12} - (\sigma/r)^{6}], \tag{1}$$

where ϵ and σ set the scale of energy and length, whereas $\tau_0 = (m\sigma^2/\epsilon)^{1/2}$ sets the scale for time with m as the mass of the particles. We use $\epsilon = \sigma = \tau_0 = 1$ without loss of generality. The phase diagram of this system as obtained from an earlier Monte Carlo study [9] is shown in Fig. 1 in the scaled temperature T–number density ρ plane. First-order liquid-solid and gas-solid boundaries are shown. In Fig. 1 we have also shown the ρ and T values at which we have obtained our results from equilibrated configurations. All our state points lie in the single phase region where one always obtains an equilibrium triangular solid. Data showing any evidence of local melting of the solid are discarded.

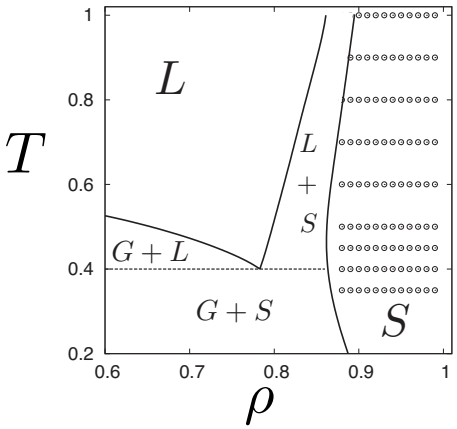

FIG. 1. Phase diagram of 2D Lennard-Jones solid as given in [9]. The first-order boundaries are shown by solid lines. Open circles indicate the T and ρ values at which we have performed MD simulations.

*tamoghna@bose.res.in
†camss@iacs.res.in
‡madan@ncbs.res.in

The main results of this paper are summarized below:

(1) We show that there is a significant fraction of nonaffine droplets in a 2D solid as the density is reduced; the fraction of particles in droplets reaches about 20% at melting.

(2) The droplets are characterized by density and excess pressure over the solid, with positive excess pressures associated with string-like droplets and negative ones associated with compact droplets.

(3) The density fluctuations of the droplets obey a distinct fluctuation-response relation associated with the susceptibility of the droplet.

(4) The excess pressure of a droplet of a given size, as we move across the phase diagram, depends on the shape of the droplets and is a nonmonotonic function of the density at low temperatures. At high temperatures, this increases monotonically with density.

(5) Finally, we show that the equal and unequal time density correlations within the droplets are liquidlike for the compact and glassy for the stringlike droplets.

Taken together, these results suggest that the nonaffine droplets should be viewed as fluctuations arising from nearby metastable liquid and glassy minima. The rest of the paper is organized as follows. In the next section we give details of our MD simulations and the data analysis scheme we use to identify nonaffine droplets. We next describe our results for the droplet shape, local thermodynamics, and density correlations. Finally, we discuss the significance of our results and conclude.

II. SIMULATION AND DATA ANALYSIS

Our MD simulations are carried out both in the canonical *NVT* and microcanonical *NVE* ensembles using a velocity Verlet algorithm [10] with a time step of 10^{-4}. Starting from a system of 10^4 particles arranged in a regular triangular lattice at desired $\rho=N/V$, we have chosen the initial velocity of each particle from a Maxwell-Boltzmann distribution at temperature T. We equilibrate the system at T for an initial 2×10^5 MD time steps. We then switch to a constant *NVE* ensemble and collect data for another 10^5 MD time steps, storing configurations at regular intervals. For our system, fluctuations of T are of order 1 in 10^{-4}. At a fixed T and ρ we analyze configurations of particles using a local measure for nonaffineness (χ) defined as the residual deformation of a region Ω surrounding a particle that is left over after fitting the best affine strain measured with respect to the ideal triangular lattice at T,ρ [8]. The neighborhood Ω, defined using a cutoff distance Λ and consisting of n particles, centered at any tagged particle 0 at $\mathbf{r}$ in the initial configuration is compared with that of the same particle at time t. We obtain the local strain ϵ_{ij} which maps as nearly as possible all the n particles from the initial to the instantaneous configuration at t. This is done by minimizing the (positive) scalar quantity,

$$\chi_\Omega(\mathbf{r},t)=\sum_{n\in\Omega}\sum_i\left\{r_n^i(t)-r_0^i(t)-\sum_j(\delta_{ij}+\epsilon_{ij})[r_n^j(0)-r_0^j(0)]\right\}^2, \quad (2)$$

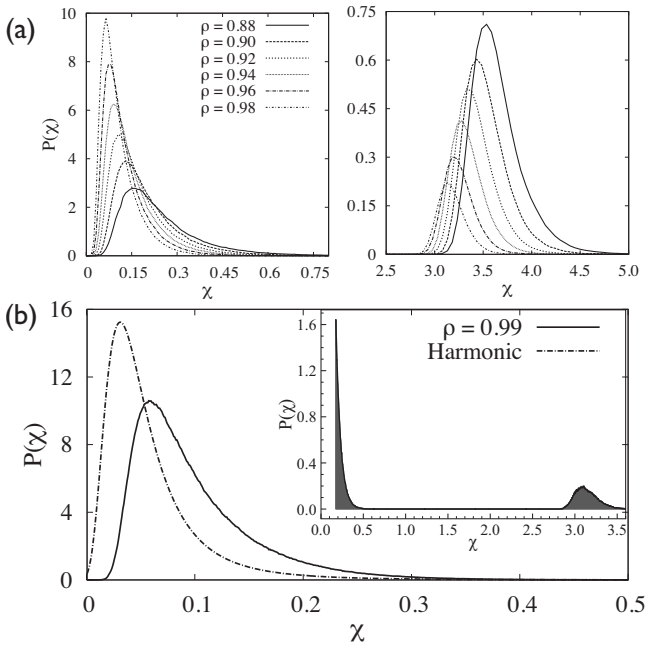

FIG. 2. (a) Probability distribution of the nonaffine parameter χ for $T=0.4$ at several densities. For these values of ρ, $P(\chi)$'s are bimodal; the contribution to the first peak is shown on the left and for the second peak it is shown on the right (note change of scale). (b) Comparison of $P(\chi)$ with that of a harmonic solid $P_{harm}(\chi)$. (Inset) Plot of $P_{\text{drop}}=P(\chi)$ for $\chi>\chi_0$ and zero otherwise.

with respect to ϵ_{ij}. Here, the indices i and $j=x,y$ and $r_n^i(t)$ and $r_n^i(0)$ are the ith component of the position vector of the nth particle in the initial and instantaneous configurations, respectively. Any *residual* value of $\chi_\Omega(\mathbf{r},t)$, which has units of σ^2, is a measure of *nonaffineness*. We have chosen $\Lambda=2.5$ as our coarse-graining length. We compute the probability distribution $P(\chi)$ [Figs. 2(a) and 2(b)] of the coarse-grained χ.

Explicit calculations show that χ is large near defects such as vacancies and dislocations which result in a change in local coordination. For $\rho>1.0$, where the solid is expected to be almost harmonic, $P(\chi)$ shows a single peak for $\chi\leq1.0$ [11]. As the density of the system is decreased, this peak becomes shorter and broader, and a second peak emerges for $2.5\leq\chi\leq5.0$. This second peak becomes more prominent as the system approaches the liquid-solid phase boundary. Inspection of the configurations of the particles with large χ values contributing to the second peak in $P(\chi)$ shows that these typically represent changes in the local topology where a pair of particles from the next-near-neighbor shell becomes closer than their nearest neighbors, thereby increasing the local density.

To identify the truly anharmonic droplet fluctuations at given ρ and T, we need to subtract out contributions to χ coming from purely harmonic distortions. In order to do this we note that for a harmonic solid, $P(\chi)$ is unimodal and has a scaling form $P(\chi;T,\rho)=P(\chi k/\Lambda^2k_BT\rho)$, where k is the spring constant of the harmonic solid. The spring constant of the reference harmonic solid was chosen to match the probability distribution of the lattice parameter in the LJ solid, obtained from the curvature of the first peak in the (angle

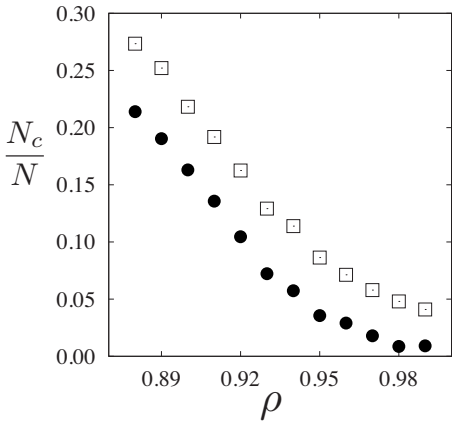

FIG. 3. Plot of the fraction N_c/N of particles in nonaffine droplets as a function of ρ. The open symbols correspond to all the nonaffine particles based on the threshold criterion described in Fig. 2(b), while the filled symbols correspond only to particles with value of χ within the second peak in $P_{\text{drop}}(\chi)$.

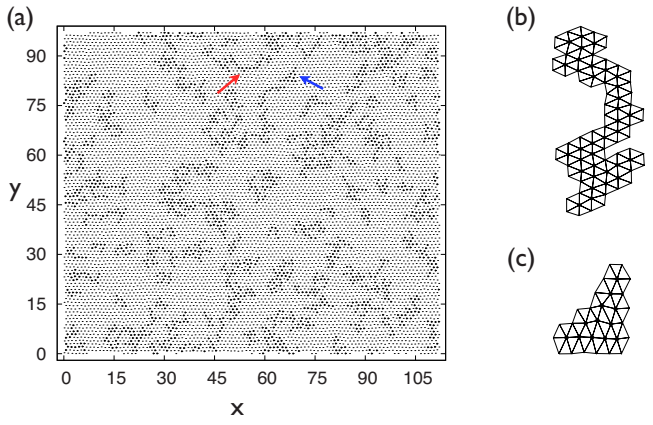

FIG. 4. (Color online) (a) Snapshot of a typical particle configuration in the LJ solid at $T=0.4$ and $\rho=0.92$. The black filled circles denote nonaffine particles, while the rest of the particles are dots (see text). Stringlike and compact droplets are pointed out using red/light gray and blue/dark gray arrows, respectively. Closeup of (b) stringlike and (c) compact droplets showing triangulated neighborhoods. While defining droplets, we also include the nearest-neighbor shell around every nonaffine particle. This spatial coarse graining improves statistics.

averaged) pair distribution function $g(r)$ of the solid. The probability distribution of χ of the equivalent harmonic solid $P_{harm}(\chi)$ was multiplied by a constant until the area of the curve matched the area of the first peak of $P(\chi)$. This procedure yields a threshold χ_0 above which there is no nonaffineness in the reference harmonic solid, and therefore any nonaffineness in the LJ solid above this value must necessarily be attributed to anharmonic fluctuations. This subtraction scheme results in the distribution $P_{\text{drop}}(\chi)$ of purely equilibrium droplet fluctuations in a solid at constant ρ and T [Fig. 2(b), inset].

III. RESULTS

We have used the above definition of nonaffine particles to carry out the rest of our analysis. The fraction of particles in droplets N_c/N is typically small but increases with decreasing average density, reaching approximately 20% close to melting [2] (see Fig. 3). This might seem too large at first; however, note that this is consistent with typical dislocation densities in 2D solids close to melting [12,13]. We expect this droplet fraction to be much lower in three dimensions.

A. Droplet size and shape

The droplets have a distribution of sizes, shapes, density, and internal pressure; we compute these quantities using standard cluster counting techniques and local Delaunay

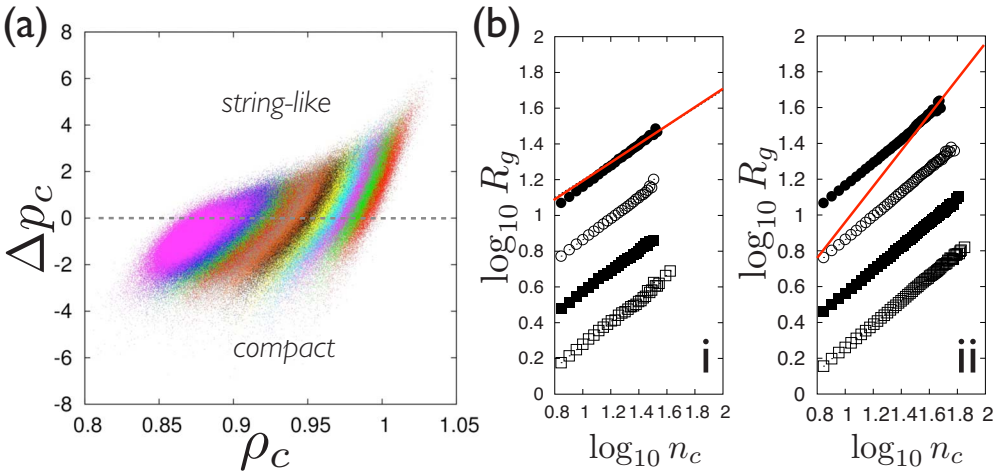

FIG. 5. (Color online) (a) Excess pressure Δp_c vs density ρ_c of the clusters as a scatter plot at densities $\rho=0.88-1.0$ shown in different colors (shades of gray). Inspection of the individual droplets corresponding to each of the colored dots shows that for $\Delta p_c>0$ droplets tend to be stringlike, while $\Delta p_c<0$ gives rise to compact droplets. (b) The radius of gyration R_g of the droplets as a function of the number of particles in the droplets n_c for several $T=0.35$ (open squares), 0.40 (filled squares), 0.45 (open circles), and 0.50 (filled circles). The data points for $T>0.35$ have been each shifted by 1 to make them visible. Note that while $R_g \sim n_c^{1/2}$ for (i) $\Delta p_c<0$ it is linear for droplets with (ii) $\Delta p_c>0$ shown in each case by solid red/dark gray lines.

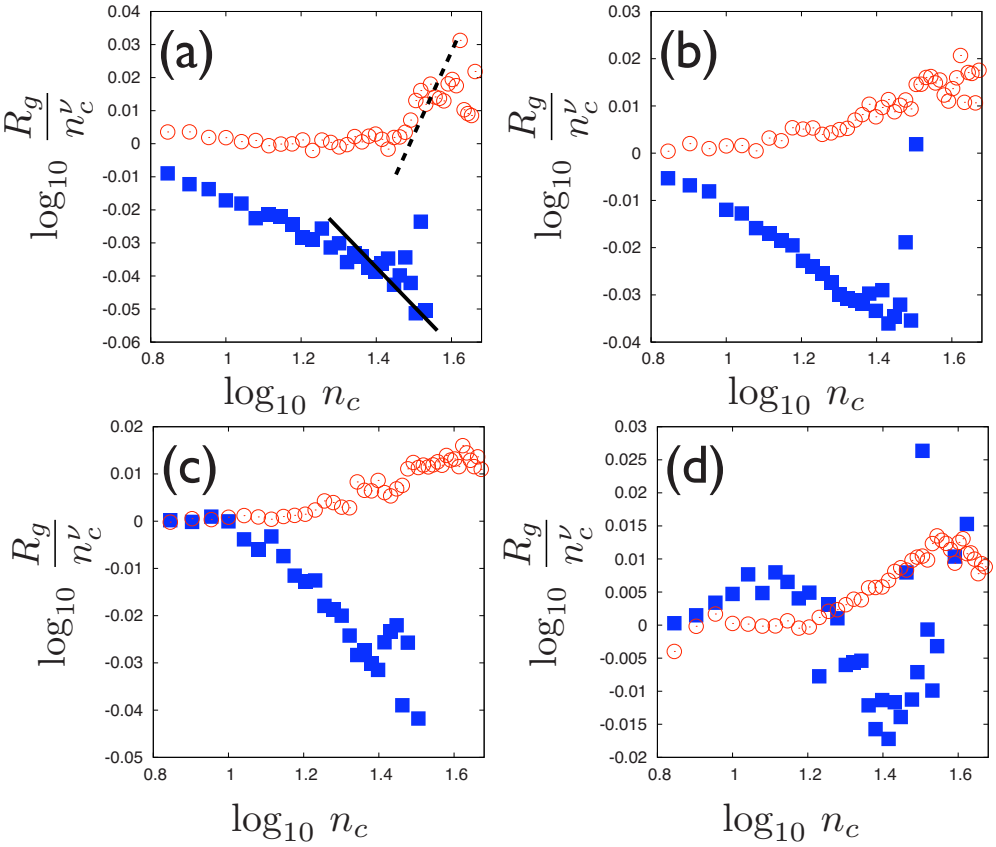

FIG. 6. (Color online) (a)–(d) Scaling plots of $\log_{10} R_g/n_c^\nu$ vs $\log_{10} n_c$ for $+ve$ (red circles) and $-ve$ (blue squares) values of Δp_c at four different temperatures $T=0.35$ (a), 0.40 (b), 0.45 (c), and 0.50 (d). We have used $\nu=0.64$, the value appropriate for (branched polymer) lattice animals in two dimensions. For small n_c, R_g/n_c^ν goes to a constant value, whereas for larger n_c it crosses over to two separate asymptotic forms depending on the sign of Δp_c. In (a) we have also shown the expected asymptotic behavior for compact (solid line) and stringlike (dashed line) droplets. For large n_c we have less statistics and therefore larger errors. As T increases, the difference between the two asymptotic forms becomes less distinct.

analysis [14]. The number of particles in the droplets n_c is exponentially distributed with a mean that increases toward the liquid-solid phase boundary.

In Fig. 4(a) we have shown a typical snapshot of the LJ particles for $\rho=0.92$ and $T=0.4$. To eliminate unimportant random fluctuations we show only droplets with $n_c>7$. The snapshots show both compact and stringlike morphologies. The droplets are dynamic; they coalesce and dissociate while continuously fluctuating in shape and size.

To understand shape and size fluctuations of the droplets we need to obtain local densities and pressure. We do this by constructing a local Delaunay net [14] of nearest-neighbor particles [see Figs. 4(b) and 4(c)]. The area of the droplet A_c is then the sum of the areas of the Delaunay triangles and the density $\rho_c \equiv n_c/A_c$. To obtain the internal pressure of the droplet, p_c, we compute the virial $\langle \mathbf{F}_{ij} \cdot \mathbf{r}_{ij} \rangle$, where $\mathbf{F}_{ij}$ and $\mathbf{r}_{ij}$ are the nearest-neighbor forces and distances, respectively, for particles i and j belonging to the droplet. The average $\langle \cdots \rangle$ is over all the particles n_c in the droplet. The droplets are characterized by a distribution of ρ_c and excess pressures, $\Delta p_c \equiv p_c - p$, where p is the mean pressure of the surrounding solid. Figure 5(a) shows a scatter diagram of the excess pressure versus the density in the cluster. We find that the droplets with high ρ_c (hence large χ) and large (positive) Δp_c are stringlike, whereas droplets with low ρ_c and $\Delta p_c<0$ are compact [Fig. 5(a)]. To study the behavior between these two extremes, we argue that these drops resemble 2D lattice animals with excess pressure [15,16]. This analogy suggests that the mean radius of gyration $R_g(n_c, \Delta p_c, T)$ obeys a crossover relation,

$$R_g^2 = n_c^{2\nu} F(\bar{p} n_c^{2\nu}), \tag{3}$$

where $\bar{p}=\Delta p_c \sigma^2/k_B T$. Note that our sign convention for the pressure implies that $\bar{p}>0$ corresponds to *deflated* droplets. Further note that in [15] the number of boundary particles is kept fixed which is a different ensemble from ours where the total number of particles in the droplets n_c is fixed.

The crossover scaling function asymptotes to $F(x \to 0) = \text{const}$ and $F(x \to \pm\infty) = x^{\theta_\pm}$. The scaling form takes into account the natural scaling $\bar{p} \sim A_c^{-1} \sim R^{-2}$, where A_c is the area of the droplet. As $x \to 0$ (i.e., small $\bar{p}$ and/or n_c) we expect that the droplet is a branched polymer with $\nu=0.64$ in two dimensions [17]. This expectation is also borne out by the particle snapshot shown in Fig. 4. The exponents $\theta_\pm$ take values such that $R_g \sim n_c$ for $x \to \infty$ (stringlike) and $R_g \sim n_c^{1/2}$ for $x \to -\infty$ (compact). In Fig. 5(b), panels (i) and (ii), we have plotted R_g vs n_c for four values of T. In each case we

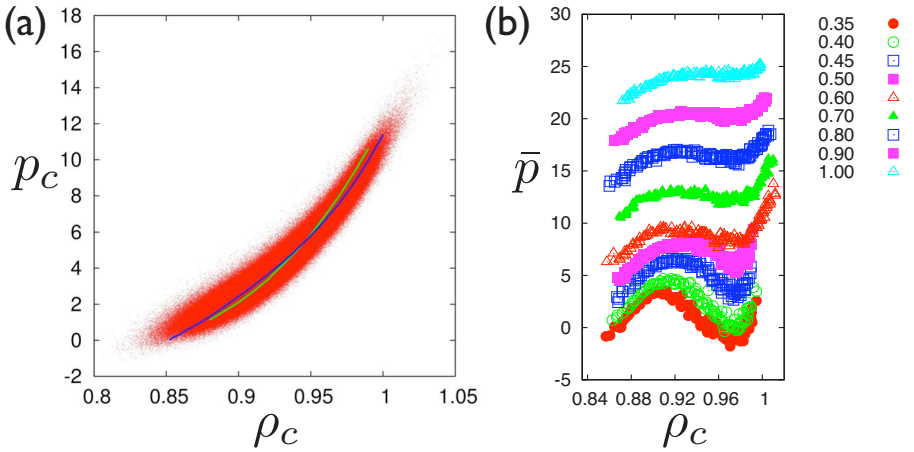

FIG. 7. (Color online) (a) Scatter plot of p_c vs ρ_c of the droplets at $T=0.40$ [red (gray) dots, the same data as in Fig. 5(a)] whose mean shows a dependence similar to an equation of state (green/light gray curve). The equilibrium equation of state of the solid is shown as a blue/dark gray curve for comparison. (b) The scaled excess pressure $\bar{p}$ as a function of mean density $\bar{\rho}_c$ for $n_c=20$ particle clusters for $T=0.35-1.0$ in different colors (and symbols). The data for $T>0.35$ have each been shifted by 4 for a unit increase in T to make them visible. Note the prominent loop showing two distinct branches at low temperatures, which disappears as T increases. We have obtained similar data for other values n_c.

have carried out a restricted average of the data separately over (i) $\Delta p_c<0$ and (ii) $\Delta p_c>0$ to improve statistics. We have also plotted, in the same graph, the expected asymptotic dependence showing that our data are consistent with Eq. (3). Unfortunately, the lack of sufficient statistics for clusters with large n_c prevents us from making a full comparison of the scaling predicted by Eq. (3) in the form of, say, a data-collapse plot [15]. To obtain better statistics one needs to simulate yet larger systems for much longer times. Nevertheless, the crossover to asymptotics is illustrated in Fig. 6 where the data in Fig. 5(b) are replotted after factoring out the small n_c branched polymer behavior. As T increases, the crossovers appear at larger n_c. Therefore, the exponents do not reach their expected asymptotic values even for the largest droplets available ($n_c \sim 10^2$), although the trends away from their $x \to 0$ limit are readily apparent,

B. Local thermodynamics of droplets

The scatter diagram in Fig. 5(a) suggests that there might be a thermodynamic interpretation of the local density and pressure of the droplets. In a bulk solid, local thermodynamic equilibrium demands that the local variations in the density are related to the pressure computed from the variation $\partial F/\partial\rho$ of the Helmholtz free energy F with respect to the density via the equation of state (EOS) of the solid at the ambient temperature. Further, within linear response, the generalized susceptibility G obtained from the slope of the EOS is related to the $q=0$ component of the equal time correlation function $k_BTG(\mathbf{q}=0)=C(\mathbf{q}=0,\ t=0)=\int d\mathbf{r}\langle\delta\rho(\mathbf{r}+\mathbf{x})\delta\rho(\mathbf{x})\rangle$, where $\delta\rho$ is the deviation from the mean density [18]. We check whether analogous thermodynamic relations hold for the droplets taken as a subsystem in contact with the rest of the solid. We want to see how far these thermodynamic considerations apply to our configurations of droplets, with the caveat that these averages are over a restricted ensemble and therefore do not affect the equilibrium thermodynamics of the bulk solid.

For fixed ρ and T for the solid, the density ρ_c and pressure p_c of the droplets are shown as a scatter plot in Fig. 7(a). The averaged curve [green (light gray) line in Fig. 7(a)] has a locus, $\bar{p}_c$ vs $\bar{\rho}_c$, which is distinct from the EOS of the equilibrium solid [blue (dark gray) line in Fig. 7(a)].

A plot of the scaled excess pressure $\bar{p}$ with the mean droplet density $\bar{\rho}_c$ [Fig. 7(b)] for a fixed particle number n_c shows a prominent nonlinear feature akin to a van der Waals loop in the equilibrium pressure-density curve at a typical first-order transition, say, between gas and liquid. The two

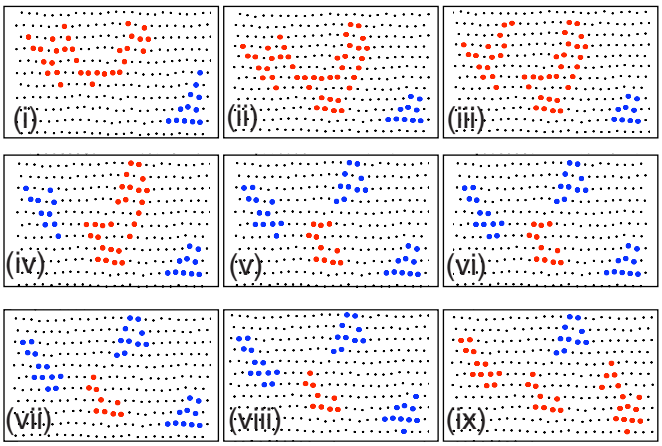

FIG. 8. (Color online) Snapshots for $T=0.4$ and $\rho=0.92$ at 0, 100, 150, 200, 250, 300, 350, 360, and 370 MD steps [(i)–(ix)] of a portion of our simulation cell showing the dynamics of two chosen droplets. The colors red (light gray) and blue (dark gray) denote $+ve$ and $-ve$ excess pressures, respectively. Note that stringlike droplets have $\Delta p_c>0$, while relatively compact droplets have $\Delta p_c<0$. Note also the dissociation of a (red/light gray) stringlike droplet into a (blue/dark gray) compact and a smaller (red/light gray) stringlike droplet [(iv)→(v)].

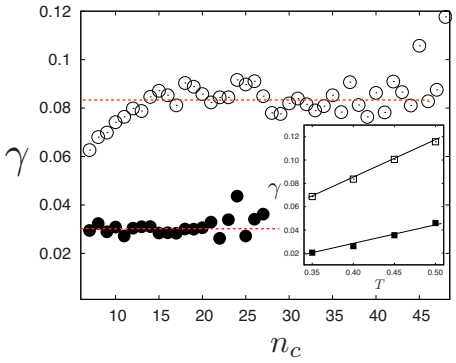

FIG. 9. (Color online) The fluctuation-response ratio γ shown as a function of n_c for droplets with $+ve$ (filled circles) and $-ve$ excess pressures; $\bar{p}$ is independent of n_c, with an intercept $\propto T$. We verify this by plotting the intercept versus T for all the droplets (inset) for $T \leq 0.5$. The filled and unfilled squares correspond to the $+ve$ and $-ve$ $\bar{p}$ branches, respectively.

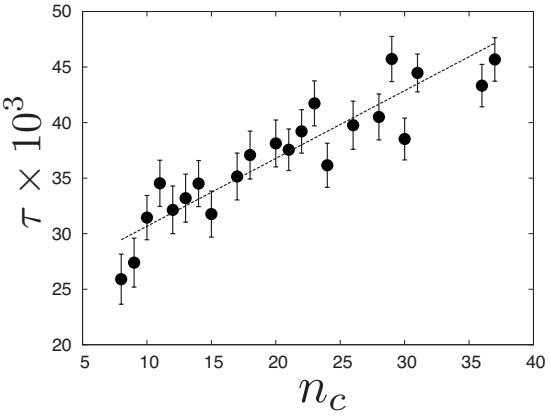

FIG. 10. Lifetime τ vs n_c for droplets at $\rho=0.92$ and $T=0.4$. Larger droplets survive longer. Note that the error bars, which are approximate and same for all the points, show the typical variation in lifetimes obtained from the width of the distribution of τ. Errors are difficult to estimate for droplets with large n_c due to the lack of sufficient statistics and may be larger than shown. The dashed straight line is a guide to the eye.

branches in the curves shown in Fig. 7(b) correspond to compact (liquidlike) and stringlike (glassy) droplets as discussed above. Integrating this pressure-density curve at fixed n_c gives the work done by thermal fluctuations in creating a droplet of size n_c. We find that at low temperatures, large excess pressure tends to convert compact droplets to stringy ones and vice versa (Fig. 8) over a characteristic relaxation time. Droplets are also seen to dissociate into distinct stringlike and compact fragments with appropriate values for the excess pressure. Quite analogous to the familiar gas-liquid transition, this metastable "van der Waals loop" vanishes at higher temperatures beyond a "critical point" which exists somewhere in the range $T=0.9-1.0$. Above this temperature the distinction between compact and stringlike droplets disappears. We find that the generalized susceptibility G obtained from the slope of $\partial\bar{p}_c/\partial\bar{\rho}_c$ is *proportional* to fluctuations of the density $\langle \delta\rho_c^2 \rangle = \langle (\rho_c - \bar{\rho}_c)^2 \rangle$, where $\langle \cdots \rangle$ denotes a time average. The fluctuation-response ratio $\gamma = \langle \delta\rho_c^2 \rangle n_c / (\rho_c^2 \partial\bar{p}_c/\partial\bar{\rho}_c)$ should be independent of n_c, with an intercept which should be proportional to the temperature T. This is shown in Fig. 9 where γ for the $+ve$ and $-ve$ $\bar{p}$ branches in Fig. 7(b) are shown separately using filled and open circles, respectively. While γ is indeed a constant, the intercept plotted versus T for all the droplets for the two branches is approximately linear in T. This is the metastable analog of the equilibrium fluctuation-response relation discussed above, suggesting that the droplets are fluctuations from a metastable state describable by a free-energy functional.

C. Density correlations

We now study density correlations within each droplet to further characterize compact and stringlike droplets. Note that these droplets have a finite lifetime $\tau(n_c)$; a plot of τ vs n_c for fixed ρ and T is shown in Fig. 10. To obtain τ, we have collected the times each constituent particle continues to belong to a droplet. As the droplet fluctuates, particles from the periphery continuously attach to and detach from the droplet leaving a set of particles at the core intact. This is clear from the snapshots shown in Fig. 4. We define τ as the persistence time of these core particles. Our analysis for different $\bar{p}$'s shows that the dense stringy clusters live longer. To obtain good statistics for the equal and unequal time density correlators, we therefore need to look at large and long-lived droplets. Figure 11 shows the equal time density correlations $g(r)$. First of all $g(r)$'s in both branches show features associated with an amorphous structure with a first peak value which is much reduced from that of the full solid. Note that while the low-density droplets are more liquidlike with smoothened peaks, the high-density droplets are glassy showing a prominent split second peak. We have also computed the self-part of the Van Hove correlation functions $G_s(t) = \langle \rho(0,0)\rho(0,t) \rangle$. This is shown in Fig. 12. While $G_s(t)$ relaxes exponentially for the low-density liquidlike droplets, the high-density droplets show non-Debye relaxation. We show that as the lifetime of the droplets increases, a prominent β-relaxation-type plateau begins to develop. This, however, gets cut off by the finite lifetime of the droplets in the solid.

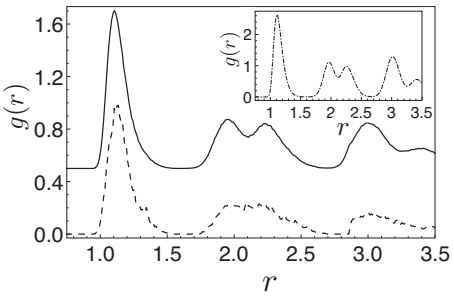

FIG. 11. Typical pair distribution function $g(r)$ for particles in nonaffine droplets at $\rho=0.88$ and $T=0.40$, drawn separately for $\Delta p_c > 0$ (solid line) and $\Delta p_c < 0$ (dashed line). $g(r)$ for the high-density droplet has been shifted by 0.5 to make it visible. Both $g(r)$'s show less crystalline structure than the solid (inset).

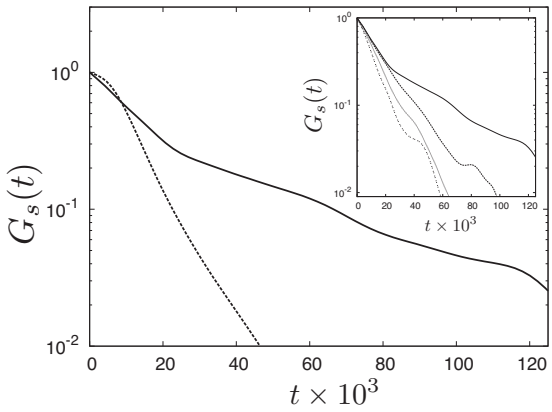

FIG. 12. The self-part of the Van Hove function $G_s(t)$ as a function of time for the same droplets whose $g(r)$ is given in Fig. 11. Note the prominent plateau for the high-density droplets, which is cut off by the finite lifetime of the droplet. Inset: development of the plateau in $G_s(t)$ with the lifetime of the droplets over which $G_s(t)$ is averaged [lines with mean τ from 50 (bottom) to 200 (top) $\times 10^{-3}$ LJ units].

IV. DISCUSSION AND CONCLUSIONS

We have shown in this paper that the excitations of an equilibrium solid at high temperatures can be interpreted as arising from a distribution of nonaffine droplets whose mean size and lifetime increase as one approaches the liquid-solid phase boundary. These droplets are characterized by density, internal pressure, and shape. The shape of the droplets crosses over from being compact to stringlike as the density increases. The observed relationship between the local pressure and density of the droplets in the form of an "equation of state" and the fluctuation-response relation of the local density strongly suggests that these nonaffine droplets arise as fluctuations from a metastable liquid or glass. Consistent with this we find that the high-density droplets have a $g(r)$ and a Van Hove function resembling that of glasses. Our main concern in this paper has been to provide evidence that droplet fluctuations of metastable liquid or glass exist in a crystalline solid and to characterize their shapes and local thermodynamic parameters. How do these fluctuations influence the properties of solids? We hope to systematically study and answer this question in the future. Some of the specific areas where the impact of droplet fluctuations may be observable are discussed below.

For example, we wonder whether our results hint at the presence of a metastable liquid-glass critical point. While Fig. 7(b) is certainly suggestive, we must remember that the size of the nonaffine droplets is typically small with $n_c \sim 100$ even for the largest droplets. A careful finite-size scaling analysis needs to be carried out in order to determine whether this feature survives for larger droplet sizes. The nature of the melting transition in the two-dimensional LJ system remains unclear in spite of being the subject of many investigations [9,19–21] over several decades. Early simulations obtained first-order liquid-solid and gas-solid transitions with prominent coexistence regions [9,19]. While at low temperatures near the triple point ($T=0.4$), one obtains a first-order melting transition [19]; at higher temperatures ($T \sim 1$) one obtains a much reduced coexistence region [20] with some characteristics of continuous [22] melting. At still higher temperatures, the melting transition appears to be unequivocally driven by dislocation unbinding [21]. Exactly how and at what temperature one obtains this change in the nature of melting is, as yet, unknown. While we do not address this question in the present paper, we speculate that droplet fluctuations may have a strong influence on the dynamics of melting. The presence of metastable critical points is known to crucially influence the dynamics of first-order transitions, e.g., the important problem of protein crystallization [23,24].

We expect these nonaffine droplets to also play an important role in the rheology of solids under applied stresses; our preliminary work in this direction is consistent with this expectation. We would also like to inquire whether it is possible to observe these droplet excitations in a real experimental situation in two and three dimensions. Such excitations, if they exist, may be difficult to disentangle from the contributions coming from a density of dislocations and grain boundaries. Perhaps direct visualization of droplet fluctuations in colloidal crystals is the best way to study these effects [25].

ACKNOWLEDGMENTS

We thank A. Paul, S. Yip, P. Sollich, T. Egami, C. Chakraborty, M. Falk, F. Spaepen, and C. Dasgupta for discussions and critical reading of the manuscript. S.S. and M.R. are pleased to acknowledge the Kavli Institute for Theoretical Physics where part of this research was performed and was supported in part by the National Science Foundation under Grant No. PHY05-51164.

[1] L. D. Landau and E. M. Lifshitz, *Theory of Elasticity*, 3rd ed. (Pergamon, New York, 1986).
[2] T. Egami, S. J. Poon, Z. Zhang, and V. Keppens, Phys. Rev. B **76**, 024203 (2007).
[3] M. H. Cohen and G. S. Grest, Phys. Rev. B **20**, 1077 (1979).
[4] A. S. Argon, Acta Metall. **27**, 47 (1979).
[5] F. Spaepen, Acta Metall. **25**, 407 (1977).
[6] For reviews see, K. Binder, Rep. Prog. Phys. **50**, 783 (1987); V. I. Yukalov, Phys. Rep. **208**, 395 (1991).
[7] D. A. Huse and D. S. Fisher, Phys. Rev. B **35**, 6841 (1987); C. Tang, H. Nakanishi, and J. S. Langer, Phys. Rev. A **40**, 995 (1989); J. S. Langer, Ann. Phys. (N.Y.) **281**, 941 (2000).
[8] M. L. Falk and J. S. Langer, Phys. Rev. E **57**, 7192 (1998).
[9] J. A. Barker, D. Henderson, and F. F. Abraham, Physica A **106**, 226 (1981).
[10] D. Frenkel and B. Smit, *Understanding Molecular Simulations* (Academic, San Diego, 2002).
[11] K. Franzrahe, P. Nielaba, and S. Sengupta, Phys. Rev. E **82**,

016112 (2010).
[12] B. Joós, in *Dislocations in Solids*, edited by F. R. N. Nabarro and M. S. Duesbery (Elsevier, Amsterdam, 1996), Vol. 10, Chap. 55, pp. 505–594.
[13] S. Sengupta, P. Nielaba, and K. Binder, Phys. Rev. E **61**, 6294 (2000).
[14] We have used the GEOMPACK code downloaded from http://people.sc.fsu.edu/~jburkardt/f_src/geompack1
[15] S. Leibler, R. R. P. Singh, and M. E. Fisher, Phys. Rev. Lett. **59**, 1989 (1987).
[16] A. C. Maggs, S. Leibler, M. E. Fisher, and C. J. Camacho, Phys. Rev. A **42**, 691 (1990).
[17] H.-P. Hsu, W. Nadler, and P. Grassberger, Comput. Phys. Commun. **169**, 114 (2005).
[18] M. Rovere, P. Nielaba, and K. Binder, Z. Phys. B: Condens. Matter **90**, 215 (1993).
[19] S. Toxvaerd, Phys. Rev. Lett. **44**, 1002 (1980).
[20] C. Udink and D. Frenkel, Phys. Rev. B **35**, 6933 (1987).
[21] K. Chen, T. Kaplan, and M. Mostoller, Phys. Rev. Lett. **74**, 4019 (1995).
[22] K. J. Strandburg, Rev. Mod. Phys. **60**, 161 (1988).
[23] P. Rein ten Wolde and D. Frenkel, Science **277**, 1975 (1997).
[24] P. Kumar, Z. Yan, L. Xu, M. G. Mazza, S. V. Buldyrev, S. H. Chen, S. Sastry, and H. E. Stanley, Phys. Rev. Lett. **97**, 177802 (2006).
[25] K. Zahn, A. Wille, G. Maret, S. Sengupta, and P. Nielaba, Phys. Rev. Lett. **90**, 155506 (2003).